International Journal of Solids and Structures 51 (2014) 1089–1102

Contents lists available at ScienceDirect

International Journal of Solids and Structures

journal homepage: www.elsevier.com/locate/ijsolstr

Stability boundaries of two-parameter non-linear elastic structures

Mohamad Rezaiee-Pajand *, Behrang Moghaddasie

Department of Civil Engineering, Ferdowsi University of Mashhad, Mashhad, Iran

ARTICLE INFO

Article history:
Received 11 July 2013
Received in revised form 24 November 2013
Available online 11 December 2013

Keywords:
Critical point
Control parameter
Arc-length method
Stability boundary
Equilibrium path
Imperfection

ABSTRACT

The load-bearing capacity of structures can be influenced by variations in parameters, such as initial geometric defects, multi-parameter loadings, material specifications and temperature. This paper aims to introduce a new formulation to trace the stability boundaries of two-parameter elastic structures. The proposed procedure can find a set of critical points, both limit and bifurcation ones, via a modified Newton's method. In the authors' formulation, the residual force is set to zero, and a critically constraint is satisfied simultaneously. Numerical examples presented in this paper demonstrate the efficiency of the suggested method.

1. Introduction

In many structural systems, parameters, such as initial geometric defects, extra loadings and changes in temperature can significantly influence the load carrying capacity. The equilibrium path and, subsequently, the buckling strength are usually sensitive to these parameters (or imperfections). A broad class of structures, like columns, trusses, shallow arches and thin-walled structures are examples of such systems (Ikeda and Ohsaki, 2007; Parente et al., 2008). Finding a precise relationship between control parameters and the final strength of structures subjected to external loadings can be helpful for both analysts and structural designers to have better understanding about the structural behavior. In mechanical–structural problems, it is common to assume that the magnitude of imperfections varies through one or more control parameters (Huseyin, 1975). Subsequently, the equilibrium equations and the critical load(s) are dependent on these parameters.

Critical points (e.g. limit, simple bifurcation and multi-bifurcation points) play an important role in the post-buckling behavior of structures. Along tracing the equilibrium path, finding the type and the exact locus of such points is needed for choosing a suitable numerical strategy. In the literature, several techniques for the calculation of equilibrium paths are extensively discussed (Crisfield, 1983; Forde and Stiemer, 1987; Riks, 1979). Most of these numerical techniques are based on Newton's method, which gives a number of discrete equilibrium points through an incremental–iterative procedure (Chen and Blandford, 1993; Rezaiee-Pajand et al., 2009; Widjaja, 1998). Many of these techniques become divergent or choose a wrong path when they reach critical points. Previously, many efforts have been made by researchers in the area of critical points' detection (Battini et al., 2003; Seydel, 1979; Wriggers et al., 1988). Since the tangent stiffness matrix becomes singular at these points, most of the proposed methods use this characteristic as the critically constraint, which is added to the governing equations, and apply an iterative procedure to obtain the supposed critical point (Fujii and Ramm, 1997; Kouhia et al., 2012; Wriggers and Simo, 1990).

The final strength of a structure can be affected by control parameters (or imperfections), such as initial geometric defects, load imperfection and thermal stresses (Ohsaki and Ikeda, 2009; Parente et al., 2006). By simultaneously perturbing the equilibrium equations and the critically constraint in the vicinity of the critical point, the sensitivity analysis of critical states can be investigated (Godoy and Banchio, 2001; Thompson and Hunt, 1973; Wu and Wang, 1997). Although this type of method is compatible with the finite element coding, it needs the calculation of high-order derivatives of the tangent stiffness matrix to obtain a better result. Furthermore, the range of validity is restricted in the vicinity of the critical point. The Lyapunov–Schmidt–Koiter asymptotic approach is another technique with similar advantages and disadvantages. In this process, the governing equations are regularized by a perturbation parameter (Casciaro et al., 1998; Casciaro et al., 1992, 2009; Koiter, 1945). There are also a number of techniques based on incremental–iterative procedures that directly obtain the critical point(s) of parameterized (imperfect) structures (Eriksson et al., 1999; Moghaddasie and Stanciulescu, 2013a; Wu, 2000). In such methods, the equilibrium equations and the critically

* Corresponding author. Tel.: +98 9153130340; fax: +98 511 8412912.
E-mail address: mrpajand@yahoo.com (M. Rezaiee-Pajand).

0020-7683/$ - see front matter © 2013 Elsevier Ltd. All rights reserved.
http://dx.doi.org/10.1016/j.ijsolstr.2013.12.004

constraint are simultaneously convinced via an iterative procedure. The superiority of these schemes in comparison with perturbation approaches is that errors will not increase for large values of the parameter(s).

This paper introduces a new formulation to find the relationship between the buckling strength of non-linear elastic structures and the variation in a control parameter. In this way, an incremental–iterative procedure is used to simultaneously set the residual force to zero and convince the critical constraint. This constraint deals with the critical eigenvector of the tangent stiffness matrix. *In addition, the authors propose a formula to update the spherical arc-length constraint in each increment to improve the convergence.* The suggested technique is based on Newton's method, and leads to a set of discrete critical point. Each point is directly computed from the previous one. Consequently, the suggested approach is suitable for conservative systems (e.g. elastic structure), which the locus of critical points are independent of the relative equilibrium paths. The suggested method includes the following features all together: *(a) the mode change in buckling does not lead to divergence; (b) errors will not increase for large magnitudes of control parameters; (c) both limit and simple bifurcation points can be detected; (d) the convergence properties are not sensitive to variations in the stiffness matrix; and (e) since each critical point is directly calculated from the previous one, globalization techniques (which are necessary for the computation of the critical point from the unloaded state) are not needed to use for structures with large pre-critical displacements.* Applying a globalization technique is crucial when the current state is far from the desired critical point, and make the method convergent (see, for example, (Dennis Jr. and Schnabel, 1996)).

In the following, a brief outline for the paper is given: Section 2 provides some basic equations for tracing the equilibrium path. In addition, the spherical arc-length is briefly described. In Section 3, the characteristics of critical states are investigated, and a classification of simple critical points is introduced. Moreover, an iterative procedure for calculating the critical load from the unloaded state is presented. Section 4 defines the concept of stability boundary in parameterized systems. The formulation and the numerical implementation of the proposed method for parameter sensitivity analysis of critical points are given in this section. Numerical examples in Section 5 examine the accuracy and computational efficiency of the suggested procedure in tracing critical points with different types of control parameters and imperfections. Finally, concluding remarks are presented in Section 6.

2. Equilibrium path

The total potential energy Π is a function of the nodal displacement vector $\mathbf{u} \in \mathbb{R}^n$ and the load parameter $p \in \mathbb{R}$ for perfect structures. Here, n denotes the number of degrees of freedom (DoFs). This energy is a summation of internal strain energy Φ and the work done by the external load. For structures under a displacement independent loading, Π is:

$$\Pi(\mathbf{u}, p) = \Phi(\mathbf{u}) - p\,\mathbf{q}^T\mathbf{u}, \tag{1}$$

where $\mathbf{q}$ is the external load vector, and the superscript T shows the transpose of the supposed vector or matrix. In elastic structures, the value of Π is stationary for equilibrium states. Consequently, its first derivative with respect to $\mathbf{u}$, which is called residual force $\mathbf{r}$, is equal to $\mathbf{0}$, and it leads to a set of equilibrium equation as follows:

$$\mathbf{r}(\mathbf{u}, p) = \mathbf{F}_{int}(\mathbf{u}) - p\,\mathbf{q} = \mathbf{0}. \tag{2}$$

Here, $\mathbf{F}_{int}(\mathbf{u})$ represents the nodal internal force and equals $\partial\Phi/\partial\mathbf{u}$. The vector $p\mathbf{q}$ denotes the external load. The set of points satisfying Eq. (2) is called the *equilibrium path*.

In order to trace the equilibrium path, many numerical techniques have been developed and used in the literature (see, for example, (Crisfield, 1981; Krenk, 1995; Le Grognec and Le Van, 2008; Riks, 1979)). A robust scheme, which obtains a set of discrete points on the equilibrium path, is based on Newton's method. This method usually includes incremental and iterative parts. In this paper, $\Delta\mathbf{u}$ and Δp represent the nodal displacement and load increments (predictors), respectively, and their relationship is:

$$\mathbf{K}_T(\mathbf{u})\Delta\mathbf{u} = \Delta p\mathbf{q}, \tag{3}$$

where $\mathbf{K}_T$ denotes the tangent stiffness matrix and can be derived from the second derivative of the strain energy with respect to $\mathbf{u}$. In the iterative part, the increments are updated by correctors:

$$\begin{cases} \Delta\mathbf{u}_{i+1} = \Delta\mathbf{u}_i + \delta\mathbf{u}_i \\ \Delta p_{i+1} = \Delta p_i + \delta p_i. \end{cases} \tag{4}$$

The superscript i represents the iteration number within each increment. Since the incremental–iterative methods obtain a set of discrete points, an extra constraint is added to the system:

$$\begin{Bmatrix} \mathbf{r}(\mathbf{u}, p) \\ L(\mathbf{u}, p) \end{Bmatrix}_{(n+1)\times 1} = \begin{Bmatrix} \mathbf{0} \\ 0 \end{Bmatrix}_{(n+1)\times 1}. \tag{5}$$

The analyst may utilize various formulae for L. In the arc-length algorithm, the additional constraint is assumed to be an $n+1$ dimensional sphere in the space of $(\mathbf{u}, p) \in \mathbb{R}^{n+1}$ (Crisfield, 1991):

$$\alpha_u^2\Delta\mathbf{u}^T\Delta\mathbf{u} + \alpha_p^2\Delta p^2 - \Delta s^2 = 0, \tag{6}$$

where Δs is the arc-length. The parameters α_u and α_p determine the contributions of displacement and load terms in the arc-length equation. Fig. 1 shows the incremental–iterative procedure in the arc-length approach. As it can be seen, $\Delta s/\alpha_u$ and $\Delta s/\alpha_p$ represent the radii of the $n+1$ dimensional sphere in the directions of $\mathbf{u}$ and p, respectively.

If the contribution of the load term in Eq. (6) is omitted by choosing $\alpha_p = 0$, the cylindrical arc-length constraint is obtained (Crisfield, 1981; Magnusson and Svensson, 1998; Ramm, 1981). This means that the radius of the $n+1$ dimensional sphere in the direction of the load parameter becomes infinitely large. In contrast, for the choice $\alpha_u = 0$, the spherical arc-length method changes into the standard Newton–Raphson (load control) scheme. Based on Fig. 1, the values of the first increments are relative to the magnitude of the arc-length Δs, and can be calculated as follows:

$$\Delta p_1 = \pm\frac{\Delta s}{\sqrt{\alpha_u^2\mathbf{b}_0^T\mathbf{b}_0 + \alpha_p^2}}, \tag{7}$$

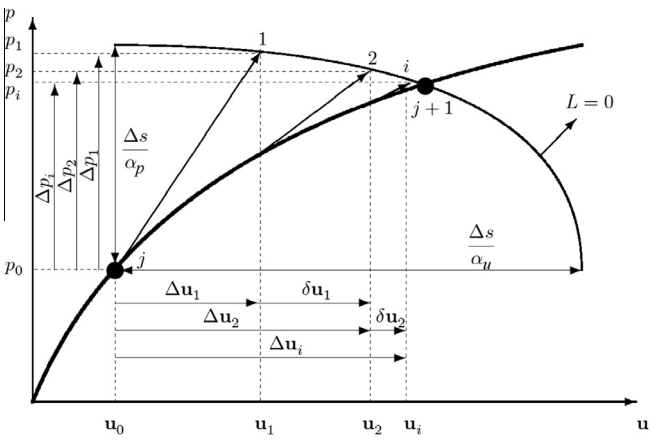

Fig. 1. Spherical arc-length procedure.

$$\Delta \mathbf{u}_1 = \Delta p_1 \mathbf{b}_0. \tag{8}$$

The converged values at the previous equilibrium point j is represented by the subscript 0. In Eq. (7), the sign which results in the smallest angle between the previous, and the current increments should be considered (de Souza Neto and Feng, 1999). Eq. (9) defines the vectors $\mathbf{a}_i$ and $\mathbf{b}_i$:

$$\begin{cases} \mathbf{a}_i = -\mathbf{K}_{Ti}^{-1}\mathbf{r}_i \\ \mathbf{b}_i = \mathbf{K}_{Ti}^{-1}\mathbf{q}. \end{cases} \tag{9}$$

The iterative correctors can be derived from the linearized form of Eq. (5):

$$\delta \mathbf{u}_i = \mathbf{a}_i + \delta p_i \mathbf{b}_i. \tag{10}$$

By substituting Eqs. (4) and (10) into this constraint, the following quadratic equation for δp_i is obtained:

$$A\delta p_i^2 + B\delta p_i + C = 0, \tag{11}$$

where

$$\begin{cases} A = \alpha_u^2 \mathbf{b}_i^T \mathbf{b}_i + \alpha_p^2 \\ B = 2\alpha_u^2 (\Delta \mathbf{u}_i + \mathbf{a}_i)^T \mathbf{b}_i + 2\alpha_p^2 \Delta p_i \\ C = \alpha_u^2 (\Delta \mathbf{u}_i + \mathbf{a}_i)^T (\Delta \mathbf{u}_i + \mathbf{a}_i) + \alpha_p^2 \Delta p_i^2 - \Delta s^2. \end{cases} \tag{12}$$

If Eq. (11) has two real roots, the one giving the smallest angle between the previous and the current increments is chosen. For the case of complex roots, the magnitude of Δs should be reduced (Crisfield, 1981, 1991), or one can use the method given by (Lam and Morley, 1992). In the iterative part, the analyst can also use the linearized form of the arc-length constraint (6):

$$2\alpha_u^2 \Delta \mathbf{u}_i^T \delta \mathbf{u}_i + 2\alpha_p^2 \Delta p_i \delta p_i = -L(\mathbf{u}_i, p_i). \tag{13}$$

By substituting the value of $\delta \mathbf{u}_i$ (which can be computed from Eq. (10) into (13)), the corrector for the load parameter δp_i is obtained (Crisfield, 1991).

3. Critical points

In the previous section, a numerical method to trace the equilibrium path is described. In the presented incremental–iterative procedure, the tangent stiffness matrix $\mathbf{K}_T$ is an important parameter for the calculation of predictors and correctors. Sudden changes in the characteristics of $\mathbf{K}_T$ can affect the convergence properties of the procedure. For instance, in some particular equilibrium points, the tangent stiffness matrix becomes singular. In the vicinity of such points, the values of $\mathbf{a}_i$ and $\mathbf{b}_i$, given by Eq. (9), become infinitely large, and subsequently, degradation of numerical robustness can be observed. These particular equilibrium points are called *critical points*. Fig. 2 displays three types of critical points: (a) limit, (b) simple bifurcation and (c) multi-bifurcation points. In limit points, the variation in the load parameter is equal to zero. The equilibrium point on the intersection of two equilibrium paths is a simple bifurcation point. Finally, more branches intersect at multi-bifurcation points.

Since sudden changes on the behavior of structures can be seen at critical points, an important issue in the analysis of non-linear structural systems is to find these points along the equilibrium path. The singularity of the tangent stiffness matrix is the constraint that distinguishes critical points from other ordinary equilibrium points. The subsequent singularity constraint could be considered:

$$|\mathbf{K}_T| = 0, \tag{14}$$

or

$$\lambda_k = 0, \quad k = 1, \ldots, h, \tag{15}$$

or

$$\mathbf{K}_T \mathbf{\Phi}_k = \mathbf{0}, \quad k = 1, \ldots, h. \tag{16}$$

Here, λ_k and $\mathbf{\Phi}_k$ denote the kth critical eigenvalue and eigenvector of $\mathbf{K}_T$, respectively. $|\mathbf{K}_T|$ is the determinant of the tangent stiffness matrix. h represents the rank deficiency of $\mathbf{K}_T$. The value of h is equal to one for limit and simple critical points and two or greater for multi-bifurcation points. In elastic structures, the tangent stiffness matrix is symmetric. As a result, all eigenvalues of $\mathbf{K}_T$ are real and its left and right eigenvectors are equal. The focus of this paper is on the analysis of limit and simple bifurcation points, which are named *simple critical points*. In the following subsection, a classification of such points is given.

3.1. Classification of simple critical points

When a critical point is detected along the equilibrium path, its type should be determined. In this way, the equilibrium path can be assumed as a curve in the space of $(\mathbf{u}, p) \in \mathbb{R}^{n+1}$, which is a function of the non-decreasing parameter s (Parente et al., 2006, 2008; Planinc and Saje, 1999). Consequently, the equilibrium equation (2) can be written in the following form:

$$\mathbf{r}(\mathbf{u}(s), p(s)) = \mathbf{0}. \tag{17}$$

For structures under a displacement independent loading, the first differentiation of Eq. (17) with respect to s leads to Eq. (18):

$$\dot{\mathbf{r}} = \mathbf{K}_T \dot{\mathbf{u}} - \dot{p}\mathbf{q} = 0, \tag{18}$$

where $(\dot{\cdot})$ represents the derivative with respect to s. Since the tangent stiffness matrix is symmetric, $\mathbf{\Phi}^T \mathbf{K}_T = \mathbf{0}$ is another form of the critical condition (16). The following relationship can be obtained by multiplication of Eq. (18) by $\mathbf{\Phi}^T$:

$$\dot{p}\mathbf{\Phi}^T \mathbf{q} = 0. \tag{19}$$

As it was mentioned previously, the variation in the load parameter is equal to zero in limit points ($\dot{p} = 0$). Therefore, Eq. (20) shows a criterion for distinguishing between limit and simple bifurcation points:

$$\begin{cases} \mathbf{\Phi}^T \mathbf{q} \neq 0 \quad \rightarrow \quad \text{limit point} \\ \Phi^T \mathbf{q} = 0 \quad \rightarrow \quad \text{bifurcation point}. \end{cases} \tag{20}$$

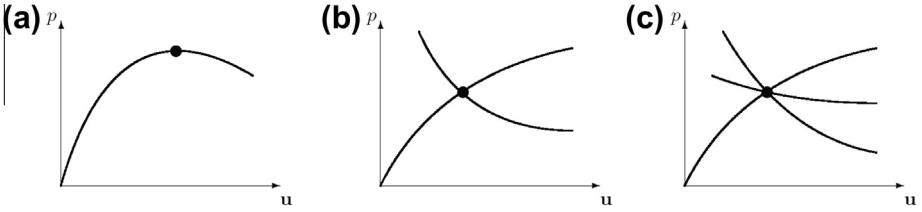

Fig. 2. Critical points: (a) limit (b) simple bifurcation (c) multi-bifurcation.

The classification of critical points is helpful in: (a) choosing a suitable numerical strategy to find the locus of such points (Eriksson et al., 1999; Lopez, 2002a,b) and (b) sensitivity analysis purposes (Ohsaki, 2005; Parente et al., 2008). This issue will be discussed later. In the following subsection, a powerful numerical procedure based on Newton's method will be described.

3.2. Direct calculation of critical points

In order to find critical points, one can use the *indirect* computation (Crisfield, 1997; Vannucci et al., 1998). In this method, a test function is defined and evaluated along tracing the equilibrium path. When the sign of this function changes from the previous equilibrium point to the current one, it reveals that a critical point has been passed. This is called the bracketing procedure. In the process of *direct* calculation of critical points, an iterative method is applied without tracing the equilibrium path. Here, a direct algorithm is investigated (Planinc and Saje, 1999; Wriggers and Simo, 1990; Wriggers et al., 1988).

As it was mentioned previously, a critical point is an equilibrium point which is simultaneously satisfying the critical condition. One may choose the constraint (16) for finding a simple critical point ($h = 1$). Consequently, the following equations should be convinced:

$$\begin{Bmatrix} \mathbf{r}(\mathbf{u},p) \\ \mathbf{K}_T(\mathbf{u})\Phi \\ l(\Phi) \end{Bmatrix}_{(2n+1)\times 1} = \begin{Bmatrix} \mathbf{0} \\ \mathbf{0} \\ 0 \end{Bmatrix}_{(2n+1)\times 1}. \tag{21}$$

$l(\mathbf{\Phi})$ is a normalizing function removing the singularity of the system (21). One choice for the normalizing is the following function (Parente et al., 2006; Wriggers et al., 1988):

$$l(\mathbf{\Phi}) = \|\mathbf{\Phi}\| - 1. \tag{22}$$

Since only one eigenvector is used, Eq. (21) is suitable for calculation of simple critical points. In the case of multi criticality ($h > 1$), h critical conditions described in (16) should be considered (Eriksson et al., 1999). The linearized form of Eq. (21) for structures under a displacement independent loading is:

$$\begin{bmatrix} \mathbf{K}_{Ti} & \mathbf{0} & -\mathbf{q} \\ \delta\mathbf{K}_{\Phi i} & \mathbf{K}_{Ti} & \mathbf{0} \\ \mathbf{0}^T & \mathbf{\Phi}_i^T/\|\mathbf{\Phi}_i\| & 0 \end{bmatrix} \begin{Bmatrix} \delta\mathbf{u}_i \\ \delta\mathbf{\Phi}_i \\ \delta p_i \end{Bmatrix} = -\begin{Bmatrix} \mathbf{r}_i \\ \mathbf{K}_{Ti}\mathbf{\Phi}_i \\ \|\mathbf{\Phi}_i\| - 1 \end{Bmatrix}. \tag{23}$$

The subscript i denotes the iteration number. The directional derivatives of the tangent stiffness matrix with respect to an arbitrary vector $\mathbf{x}$ (denoted by $\delta\mathbf{K}_\mathbf{x}$) can be evaluated by the third variation of the strain energy (see, for instance, (Casciaro et al., 1992; Garcea et al., 1999; Ibrahimbegović and Al Mikdad, 2000)) or approximately calculated by the following equation:

$$\delta\mathbf{K}_\mathbf{x} = \frac{\mathbf{K}_T(\mathbf{u}+t\mathbf{x}) - \mathbf{K}_T(\mathbf{u})}{t}, \tag{24}$$

where t is a numerical parameter and can be taken as (Battini et al., 2003; Magnusson and Svensson, 1998; Wriggers and Simo, 1990):

$$t = \max_{1\leqslant i\leqslant n}|x_i| \times \eta. \tag{25}$$

x_i is the i component of the vector $\mathbf{x} \in \mathbb{R}^n$, and η is based on the machine precision.

By considering the criterion given in (20), if the analyst wants to obtain only limit points, the next normalizing function $l(\mathbf{\Phi})$ can be assumed:

$$l(\mathbf{\Phi}) = \mathbf{\Phi}^T\mathbf{q} - 1. \tag{26}$$

It can be proven that Eq. (21) has a solution until $\mathbf{\Phi}^T\mathbf{q} \neq 0$ (Lopez, 2002a; Moore and Spence, 1980). This means the matrix described in (23) has a singularity at bifurcation points, and the approach becomes progressively ill-conditioned. To remove this singularity, considering an additional equation could be helpful (Cardona and Huespe, 1999; Eriksson, 1994; Wriggers and Simo, 1990). Here, an augmented of Eq. (21) is introduced (Lopez, 2002a,b):

$$\begin{Bmatrix} \mathbf{r}(\mathbf{u},p) + \gamma\mathbf{\Phi} \\ \mathbf{K}_T(\mathbf{u})\mathbf{\Phi} \\ \|\mathbf{\Phi}\| - 1 \\ \mathbf{\Phi}^T\mathbf{q} \end{Bmatrix}_{(2n+2)\times 1} = \begin{Bmatrix} \mathbf{0} \\ \mathbf{0} \\ 0 \\ 0 \end{Bmatrix}_{(2n+2)\times 1}, \tag{27}$$

where γ is a new added unknown, and the last equation is the property of bifurcation points. The linearized form of Eq. (27) is as follows:

$$\begin{bmatrix} \mathbf{K}_{Ti} & \mathbf{0} & -\mathbf{q} & \mathbf{\Phi}_i \\ \delta\mathbf{K}_{\Phi i} & \mathbf{K}_{Ti} & \mathbf{0} & \mathbf{0} \\ \mathbf{0}^T & \mathbf{\Phi}_i^T/\|\mathbf{\Phi}_i\| & 0 & 0 \\ \mathbf{0}^T & \mathbf{q}^T & 0 & 0 \end{bmatrix} \begin{Bmatrix} \delta\mathbf{u}_i \\ \delta\mathbf{\Phi}_i \\ \delta p_i \\ \delta\gamma_i \end{Bmatrix} = -\begin{Bmatrix} \mathbf{r}_i + \gamma_i\mathbf{\Phi}_i \\ \mathbf{K}_{Ti}\mathbf{\Phi}_i \\ \|\mathbf{\Phi}_i\| - 1 \\ \mathbf{\Phi}_i^T\mathbf{q} \end{Bmatrix}. \tag{28}$$

4. Stability boundary

Additional parameters, such as geometric defects, extra load vector and thermal stresses, can affect the load-bearing capacity of real structures. In this section, the stability boundary for conservative systems is defined. Afterwards, the authors' formulation for tracing the stability boundary is introduced. Finally, the numerical implementation of the proposed method will be given.

The total potential energy Π is stationary for equilibrium states (Choong and Kim, 2001; Huseyin, 1975; Thompson and Hunt, 1973):

$$\Pi(\mathbf{u},p,\varepsilon) = \text{Stationary}. \tag{29}$$

In comparison with Eq. (1), an additional control parameter $\varepsilon \in \mathbb{R}$ is considered in parameterized systems (e.g. imperfect structures). To derive the equilibrium equations of the system, the first derivative of Π with respect to $\mathbf{u}$ should be equal to zero:

$$\Pi_\mathbf{u}(\mathbf{u},p,\varepsilon) = \mathbf{r}(\mathbf{u},p,\varepsilon) = \mathbf{0}. \tag{30}$$

Here, $\mathbf{r}$ is the residual force, and the subscript $\mathbf{u}$ denotes the derivative with respect to the nodal displacement. Eq. (30) shows a system of n equations and $n+2$ unknowns for a structure with n DoFs. Subsequently, the manifold convincing Eq. (30) is one or more surfaces within the space of $(\mathbf{u},p,\varepsilon) \in \mathbb{R}^{n+2}$. Fig. 3 illustrates these equilibrium surfaces for a parameterized system.

Similar to perfect structures, both limit and bifurcation points can be seen on the equilibrium surfaces (Fig. 3). The constraint $\partial p/\partial\mathbf{u} = \mathbf{0}$ is satisfied at limit points; and bifurcation points are located at the intersection of equilibrium surfaces. A critical condition for both cases can be considered as follows:

$$|\Pi_{\mathbf{uu}}(\mathbf{u},p,\varepsilon)| = 0. \tag{31}$$

For structures under a displacement independent loading, $\Pi_{\mathbf{uu}}$ equals the tangent stiffness matrix $\mathbf{K}_T$. Eqs. (30) and (31) provide equations with unknowns. Consequently, the locus of critical points is a curve or a number of curves in the space of $(\mathbf{u},p,\varepsilon) \in \mathbb{R}^{n+2}$. The projection of these curves onto the plane of p and ε axes is called *stability boundary*. Actually, the relationship between load-bearing capacity and the magnitude of the control parameter can be shown by the stability boundary of structures. In the following subsection, the proposed numerical method to *directly* trace the stability

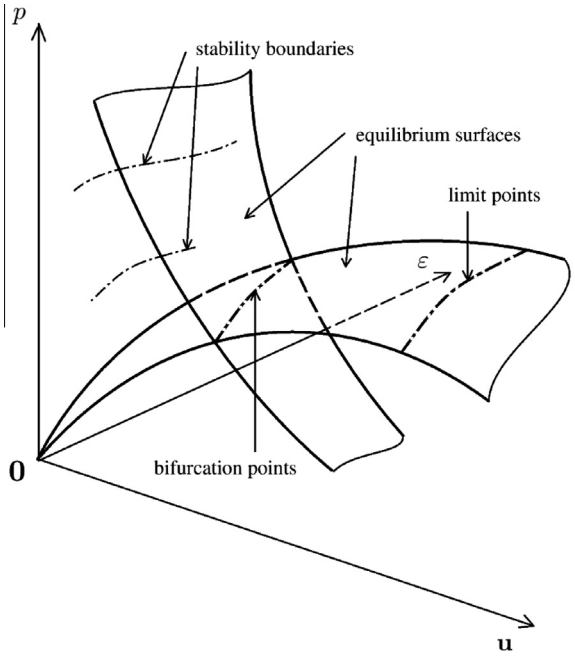

Fig. 3. Equilibrium surfaces, critical points and stability boundaries for a parameterized system.

boundary is described. This technique is based on an incremental–iterative scheme with *quadratic rate of convergence*. The suggested approach can track limit and bifurcation points for a wide range of the control parameter.

4.1. Formulation for parameterized systems

In order to trace critical points in a parameterized system through an incremental–iterative technique, the following set of equations is considered:

$$\begin{Bmatrix} \mathbf{r}(\mathbf{u},p,\varepsilon) \\ \mathbf{K}_T(\mathbf{u},\varepsilon)\boldsymbol{\Phi} \\ l(\boldsymbol{\Phi}) \\ L(\mathbf{u},p,\varepsilon) \end{Bmatrix}_{(2n+2)\times 1} = \begin{Bmatrix} \mathbf{0} \\ \mathbf{0} \\ 0 \\ 0 \end{Bmatrix}_{(2n+2)\times 1}. \tag{32}$$

The first equation represents the equilibrium state for a two-parameter system. The critically constraint is given in the second and the third equations. Since by utilizing the incremental–iterative algorithm a number of discrete points are obtained (instead of a continuous curve), an extra equation ($L = 0$) is added to the system. Here, the authors' suggestion for this equation is an $n+2$ dimensional sphere in the space of $(\mathbf{u},p,\varepsilon)\in\mathbb{R}^{n+2}$:

$$\alpha_u^2\Delta\mathbf{u}^T\Delta\mathbf{u}+\alpha_p^2\Delta p^2+\alpha_\varepsilon^2\Delta\varepsilon^2-\Delta s^2=0, \tag{33}$$

where the parameters α_u, α_p and α_ε determine the contribution of displacement, load and control parameter terms. Δs is the arc-length. By considering Eqs. (22) and (33), the linearized form of the system (32) will be as follows:

$$\begin{bmatrix} \mathbf{K}_{Ti} & \mathbf{0} & -\mathbf{q} & \mathbf{F}_{\varepsilon i} \\ \delta\mathbf{K}_{\Phi i} & \mathbf{K}_{Ti} & \mathbf{0} & \delta\mathbf{K}_{\varepsilon i}\boldsymbol{\Phi}_i \\ \mathbf{0}^T & \boldsymbol{\Phi}_i^T/\|\boldsymbol{\Phi}_i\| & 0 & 0 \\ 2\alpha_u^2\Delta\mathbf{u}_i^T & \mathbf{0}^T & 2\alpha_p^2\Delta p_i & 2\alpha_\varepsilon^2\Delta\varepsilon_i \end{bmatrix} \begin{Bmatrix} \delta\mathbf{u}_i \\ \delta\boldsymbol{\Phi}_i \\ \delta p_i \\ \delta\varepsilon_i \end{Bmatrix} = -\begin{Bmatrix} \mathbf{r}_i \\ \mathbf{K}_{Ti}\boldsymbol{\Phi}_i \\ \|\boldsymbol{\Phi}_i\|-1 \\ L_i \end{Bmatrix}. \tag{34}$$

Similar to the previous sections, it is assumed that the external load is displacement independent. The magnitudes of $\mathbf{F}_{\varepsilon i}$, $\delta\mathbf{K}_{\Phi i}$ and $\delta\mathbf{K}_{\varepsilon i}$ can be approximately computed by the subsequent equations:

$$\begin{cases} \mathbf{F}_\varepsilon = \frac{\mathbf{r}(\mathbf{u},p,\varepsilon+t)-\mathbf{r}(\mathbf{u},p,\varepsilon)}{t} \\ \delta\mathbf{K}_\Phi = \frac{\mathbf{K}_T(\mathbf{u}+t\boldsymbol{\Phi},\varepsilon)-\mathbf{K}_T(\mathbf{u},\varepsilon)}{t} \\ \delta\mathbf{K}_\varepsilon = \frac{\mathbf{K}_T(\mathbf{u},\varepsilon+t)-\mathbf{K}_T(\mathbf{u},\varepsilon)}{t}. \end{cases} \tag{35}$$

The value of the numerical parameter t is derived by Eq. (25).

The exact value of the force vector $\mathbf{F}_\varepsilon$ is available for some typical control parameters. For example, in the case of having extra loading, $\mathbf{F}_\varepsilon$ is equal to the negative of the additional load vector. $\mathbf{F}_\varepsilon$ equals a thermal force vector due to thermal stresses in members caused by variation in temperature. In the case of initial geometric defects (in structures with small strains), this vector is equivalent to a nodal force that deforms the perfect structure to the imperfect state.

By considering the first three equations of (34), one can derive the iterative part of the displacement, load parameter and eigenvector as a function of the variation in the control parameter in the following shape:

$$\begin{cases} \delta\mathbf{u}_i = \mathbf{a}_u + \delta\varepsilon_i\mathbf{b}_u \\ \delta\boldsymbol{\Phi}_i = \mathbf{a}_\Phi + \delta\varepsilon_i\mathbf{b}_\Phi \\ \delta p_i = a_p + \delta\varepsilon_i b_p. \end{cases} \tag{36}$$

Here, the reason of formulating all parameters as a function of $\delta\varepsilon$ is that in the most numerical example, the monotonically increase in the control parameter can easily draw the complex curve of stability boundary in the space of $(\mathbf{u},p,\varepsilon)\in\mathbb{R}^{n+2}$. The magnitudes of the coefficients given in Eq. (36) are as follows:

$$\begin{aligned} &a_p=(\|\boldsymbol{\Phi}\|-\boldsymbol{\Phi}^T\mathbf{a}_2\mathbf{a}_1)/(\boldsymbol{\Phi}^T\mathbf{a}_2\mathbf{b}_1),\ \ \mathbf{a}_u=\mathbf{a}_1+a_p\mathbf{b}_1,\ \ \mathbf{a}_\Phi=-\boldsymbol{\Phi}+\mathbf{a}_2\mathbf{a}_u \\ &b_p=-(\boldsymbol{\Phi}^T(\mathbf{a}_2\mathbf{c}_1+\mathbf{c}_2))/(\boldsymbol{\Phi}^T\mathbf{a}_2\mathbf{b}_1),\ \ \mathbf{b}_u=b_p\mathbf{b}_1+\mathbf{c}_1,\ \ \mathbf{b}_\Phi=\mathbf{a}_2\mathbf{b}_u+\mathbf{c}_2, \end{aligned} \tag{37}$$

where

$$\begin{aligned} &\mathbf{a}_1=-\mathbf{K}_T^{-1}\mathbf{r},\quad \mathbf{b}_1=\mathbf{K}_T^{-1}\mathbf{q},\quad \mathbf{c}_1=-\mathbf{K}_T^{-1}\mathbf{F}_\varepsilon,\quad \mathbf{d}_1=-\mathbf{K}_T^{-1}\boldsymbol{\Phi} \\ &\mathbf{a}_2=-\mathbf{K}_T^{-1}\delta\mathbf{K}_\Phi,\quad \mathbf{c}_2=-\mathbf{K}_T^{-1}\delta\mathbf{K}_\varepsilon\boldsymbol{\Phi}. \end{aligned} \tag{38}$$

By substituting the values of $\delta\mathbf{u}_i$ and δp_i into the last equation of (34), $\delta\varepsilon_i$ is obtained.

The described incremental–iterative procedure starts from the previous critical point to the next one. The first increment, which is satisfying the arc-length constraint (33), has the succeeding form:

$$\Delta\varepsilon_1=\frac{\pm\Delta s}{\sqrt{\alpha_u^2\mathbf{b}_{u0}^T\mathbf{b}_{u0}+\alpha_p^2 b_{p0}^2+\alpha_\varepsilon^2}}, \tag{39}$$

$$\Delta\mathbf{u}_1=\Delta\varepsilon_1\mathbf{b}_{u0}, \tag{40}$$

$$\Delta\boldsymbol{\Phi}_1=\Delta\varepsilon_1\mathbf{b}_{\Phi 0}, \tag{41}$$

$$\Delta p_1=\Delta\varepsilon_1 b_{p0}. \tag{42}$$

The correct sign of Δs in Eq. (39) is the one that gives the smallest angle between the previous and the current increments (Ramm, 1981). After this jump, the increments are updated at the iteration part until the convergence criterion is satisfied.

An issue that can be of the analyst interest is the contribution of displacement, load and control parameter terms. Authors' experience shows that the following choice of α_u, α_p and α_ε ensures a robust and efficient simulation:

$$\begin{cases} \alpha_u = \|\ \mathbf{b}_{u0}\|/\Delta \\ \alpha_p = |\ b_{p0}|/\Delta \\ \alpha_\varepsilon = 1/\Delta, \end{cases} \tag{43}$$

where

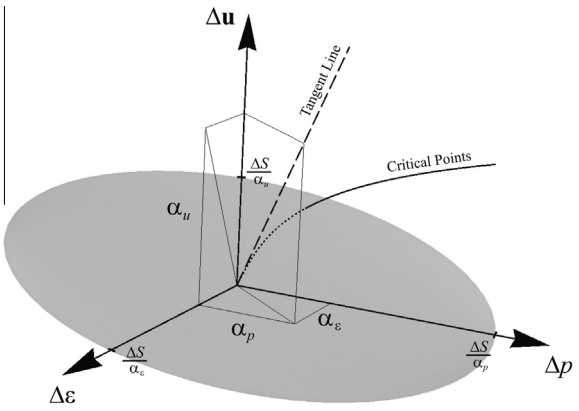

Fig. 4. Contribution of displacement, load and control parameter.

$$\Delta = \sqrt{\mathbf{b}_{u0}^T \mathbf{b}_{u0} + b_{p0}^2 + 1}. \tag{44}$$

This choice means that the contribution of each term in Eq. (33) is dependent on the cosine of the angle between the tangent of the stability boundary and the axes $\mathbf{u}$, p and ε. A smaller angle obtains a higher contribution (Fig. 4).

The authors' formulation converts the system (32) into a consistent linear form which is calculated by Newton method assuring *quadratic convergence* (Ibrahimbegović and Al Mikdad, 2000; Planinc and Saje, 1999; Wriggers et al., 1988). This property will be shown in the numerical examples. Needless to say, this linearization changes the $n+2$ dimensional sphere into a plane perpendicular to the tangent line and passing through the intersection of the line and the sphere shown in Fig. 4. Moreover, since each critical point is directly calculated from the previous one, *globalization techniques* (such as those used in (Dennis Jr. and Schnabel, 1996; Fujii and Okazawa, 1997; Fujii and Ramm, 1997)) are not needed, and the proposed methodology can trace the stability boundary for a wide range of the control parameter.

If the analyst wants to track only limit points of the structure, $l(\mathbf{\Phi})$ can be assumed as $\mathbf{\Phi}^T\mathbf{q} - 1$. By considering this assumption, which is resulting a non-zero value for the eigenvector $\mathbf{\Phi}$, and simultaneously satisfying the limit point condition (26), the coefficients a_p and b_p in Eq. (37) change into the following form:

$$\begin{cases} a_p = (1 - \mathbf{q}^T\mathbf{a}_2\mathbf{a}_1)/(\mathbf{q}^T\mathbf{a}_2\mathbf{b}_1) \\ b_p = -(\mathbf{q}^T(\mathbf{a}_2\mathbf{c}_1 + \mathbf{c}_2))/(\mathbf{q}^T\mathbf{a}_2\mathbf{b}_1). \end{cases} \tag{45}$$

As it was mentioned in the previous section, the approach becomes progressively ill-conditioned at bifurcation points (Lopez, 2002a; Moore and Spence, 1980). To overcome this problem, the system (32) should be augmented:

$$\begin{Bmatrix} \mathbf{r}(\mathbf{u},p,\varepsilon) + \gamma\mathbf{\Phi} \\ \mathbf{K}_T(\mathbf{u},\varepsilon)\mathbf{\Phi} \\ \|\mathbf{\Phi}\| - 1 \\ \mathbf{\Phi}^T\mathbf{q} \\ L(\mathbf{u},p,\varepsilon) \end{Bmatrix}_{(2n+3)\times 1} = \begin{Bmatrix} \mathbf{0} \\ \mathbf{0} \\ 0 \\ 0 \\ 0 \end{Bmatrix}_{(2n+3)\times 1}. \tag{46}$$

The linearized form of Eq. (46) is as follows:

$$\begin{bmatrix} \mathbf{K}_{Ti} & \mathbf{0} & -\mathbf{q} & \mathbf{F}_{\varepsilon i} & \mathbf{\Phi}_i \\ \delta\mathbf{K}_{\Phi i} & \mathbf{K}_{Ti} & \mathbf{0} & \delta\mathbf{K}_{\varepsilon i}\mathbf{\Phi}_i & \mathbf{0} \\ \mathbf{0}^T & \mathbf{\Phi}_i^T/\|\mathbf{\Phi}_i\| & 0 & 0 & 0 \\ \mathbf{0}^T & \mathbf{q}^T & 0 & 0 & 0 \\ 2\alpha_u^2\Delta\mathbf{u}_i^T & \mathbf{0}^T & 2\alpha_p^2\Delta p_i & 2\alpha_\varepsilon^2\Delta\varepsilon_i & 0 \end{bmatrix} \begin{Bmatrix} \delta\mathbf{u}_i \\ \delta\mathbf{\Phi}_i \\ \delta p_i \\ \delta\varepsilon_i \\ \delta\gamma_i \end{Bmatrix} = -\begin{Bmatrix} \mathbf{r}_i \\ \mathbf{K}_{Ti}\mathbf{\Phi}_i \\ \|\mathbf{\Phi}_i\| - 1 \\ \mathbf{\Phi}_i^T\mathbf{q} \\ L_i \end{Bmatrix}. \tag{47}$$

By solving the first four equations of the linear system (47), the magnitude of iterations in $\mathbf{u}$, $\mathbf{\Phi}$, p and γ corresponding to $\delta\varepsilon_i$ is obtained:

$$\begin{cases} \delta\mathbf{u}_i = \mathbf{a}_u + \delta\varepsilon_i\mathbf{b}_u \\ \delta\Phi_i = \mathbf{a}_\Phi + \delta\varepsilon_i\mathbf{b}_\Phi \\ \delta p_i = a_p + \delta\varepsilon_i b_p \\ \delta\ \gamma_i = a_\gamma + \delta\varepsilon_i b_\gamma, \end{cases} \tag{48}$$

where

$$\begin{aligned} \mathbf{a}_u &= \mathbf{a}_1 + a_p\mathbf{b}_1 + a_\gamma\mathbf{d}_1 \\ \mathbf{b}_u &= b_p\mathbf{b}_1 + \mathbf{c}_1 + b_\gamma\mathbf{d}_1 \\ a_p &= (\|\mathbf{\Phi}\|\mathbf{q}^T\mathbf{a}_2\mathbf{d}_1 + (\mathbf{a}_2\mathbf{d}_1)^T\mathbf{M}(\mathbf{a}_2\mathbf{a}_1))/\mu \\ b_p &= ((\mathbf{a}_2\mathbf{d}_1)^T\mathbf{M}(\mathbf{a}_2\mathbf{c}_1 + \mathbf{c}_2))/\mu \\ a_\gamma &= (-\|\mathbf{\Phi}\|\mathbf{q}^T\mathbf{a}_2\mathbf{b}_1 + (\mathbf{a}_2\mathbf{a}_1)^T\mathbf{M}(\mathbf{a}_2\mathbf{b}_1))/\mu \\ b_\gamma &= ((\mathbf{a}_2\mathbf{c}_1 + \mathbf{c}_2)^T\mathbf{M}(\mathbf{a}_2\mathbf{b}_1))/\mu \\ \mu &= (\mathbf{a}_2\mathbf{b}_1)^T\mathbf{M}(\mathbf{a}_2\mathbf{d}_1) \\ \mathbf{M} &= \mathbf{\Phi}\mathbf{q}^T - \mathbf{q}\mathbf{\Phi}^T. \end{aligned} \tag{49}$$

The values of $\mathbf{a}_\Phi$ and $\mathbf{b}_\Phi$ are given in Eq. (37).

The authors' formulations are also capable to be adopted for problems with more control parameters. In this way, new parameters are added to the governing equations, and the block elimination process will extend to new possible constraints. An application, which can be of interest for analysts, is the interpretation of multi-critical states. In this case, a number of critical constraints based on the rank deficiency of the tangent stiffness matrix are added to the system (46). Then, the effects of control parameters on the supposed multi-critical state are determined by using the proposed procedure.

4.2. Numerical implementation

The suggested method can obtain critical points directly from one to another. Finding the first critical point is the primary step of the analysis. Afterwards, the stability boundary is traced due to an incremental–iterative procedure. In the following, the computational steps of the proposed method are explained:

4.2.1. Finding the first critical point

The formulations corresponding to the iterative part of the proposed method can obtain the first critical point, if the starting point is sufficiently close to the critical state. To do this, a path following procedure (e.g. cylindrical arc-length method) is applied to trace the equilibrium path from the unloaded state. At the same time, a test function is defined, and its value is evaluated in each equilibrium point (Crisfield, 1997; Vannucci et al., 1998). Changes in the sign of this function (from an equilibrium point to the next one) show that a critical point has been passed. An alternative for the calculation of the first critical point is the *bracketing procedure* which is capable to find the state that the test function equals zero (Crisfield, 1997; Vannucci et al., 1998).

4.2.2. Incremental part

1. Adjusting the magnitude of Δs: The value of Δs can be chosen based on the number of iterations and the length of increments in previous steps (see, for example, (Crisfield, 1981; Krenk, 1995; Ramm, 1981)).
2. Calculation of coefficients b_{u0}, $\mathbf{b}_{\Phi 0}$ and $\mathbf{b}_{p0}$ from Eq. (37).
3. Estimation of α_u, α_p and α_ε: Eq. (43) denotes an example of possible contributions.
4. Computation of increments $\Delta\mathbf{u}_1$, $\Delta\mathbf{\Phi}_1$, Δp_1 and $\Delta\varepsilon_1$ from Eqs. (39)–(42).

4.2.3. Iterative part

1. Identifying the type of the previous critical point by considering Eq. (20): Based on the objective of the analyst, the proposed algorithms for calculation of limit or bifurcation points are chosen. If the type of critical points is not of interest for the analyst, it is better to apply Eq. (34), and for the case of ill-conditioned, Eq. (47) should be concerned.
2. Calculation of vectors and matrices $\mathbf{r}_i$, $\mathbf{F}_{\varepsilon i}$, $\delta\mathbf{K}_{\Phi i}$ and $\delta\mathbf{K}_{\varepsilon i}$.
3. Determination of $\mathbf{a}_u$, $\mathbf{b}_u$, $\mathbf{a}_\Phi$, $\mathbf{b}_\Phi$, a_p and b_p based on the type of the critical point.
4. Computation of correctors at the ith iteration.
5. Update of the increments.
6. Verifying the convergence criterion: $\|\mathbf{r}_i\| \leqslant \beta_r\|\mathbf{r}_1\|$ and $\|\mathbf{K}_{Ti}\mathbf{\Phi}_i\| \leqslant \beta_\Phi\|\mathbf{K}_{T1}\mathbf{\Phi}_1\|$ are convergence criteria used in this paper. β_r and β_Φ are the tolerances. In addition, if the number of iterations per increment reaches a specific value given by the analyst, the method is assumed to be divergent in this step, and the arc-length Δs should be reduced.

5. Numerical examples

In this section, the proposed method is examined by six numerical examples. The investigated structures are non-linear elastic, and the relationship between strains and displacements is described in terms of the Green's strains. The magnitude of the convergence tolerances β_r and β_Φ is equal to 10^{-16}. For best performance, η is assumed 10^{-64} for all examples. In each example, the value of Δs is constant for incremental steps and chosen based on the range of the control parameter. Graphical representations of the stability boundary and tabulated data with additional information are provided for the solutions.

5.1. Truss-spring system

Fig. 5 illustrates a simple truss-spring system investigated by several authors (Bergan, 1980; Krenk, 1995, 2009). The structure consists of two truss bars satisfying the theory of large displacements and rotations (Felippa, 2012), which are laterally supported by a horizontal spring. Since it is assumed that the bars are carrying only axial loads (Krenk, 1995), variation in the length of each element is the only parameter that causes axial Green's strain.

In this example, ε is an initial geometrical parameter which describes the position of the top node in the direction of z. The equilibrium path of the structure reaches a limit point when the external load P increases. The material properties and the geometry of the truss-spring system are shown in Fig. 5. Here, $k\,L/EA = 0.02$ and $h/L = 0.2$.

The ratio of P_{cr}/EA is equal to 2.741×10^{-3} for the perfect structure ($\varepsilon/h = 0$). The proposed method can find the relationship between the magnitude of the critical load and the out of plane deviation *for a wide range of the control parameter* ε. Fig. 6 illustrates the computed stability boundary. As it can be seen, the critical points calculated by (Krenk, 1995) are consistent with the result given by the suggested technique. In this example, four increments with $\Delta s = 0.08$ are used. The average number of iterations per increment is 4.5. The summaries of the computations are shown in Table 1. The quadratic convergence of the proposed procedure can be observed in this table.

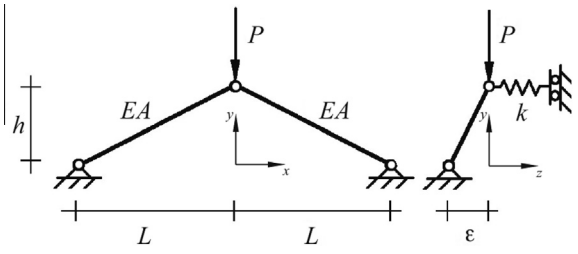

Fig. 5. Truss-spring system.

5.2. Plane truss arch

A 2D truss arch is shown in Fig. 7. The truss includes 35 bar-members and 34 degrees of freedom. Here, the truss elements satisfying the theory of large displacements and rotations are used. The axial Green's strain in each element can be evaluated by $(L^2 - L_0^2)/2L_0^2$ (Felippa, 2012). L and L_0 are the current and the initial lengths of the supposed bar, respectively. This structure is subjected to vertical loads at the top nodes. All members have the same stiffness $EA = 1.0 \times 10^7$ N. The nodal coordinates of the plane truss arch are given in Table 2.

The structure is subjected to two external load vectors. The main one is applied to half of the span, and its magnitude is a function of the load parameter P. The secondary load vector increases through the control parameter ε. For the case of perfect structure ($\varepsilon = 0$ N), $P_{cr} = 77.71$ N. The stability boundary computed by the proposed method (with $\Delta s = 9.5$) is shown in Fig. 8. In this example, all the critical points forming the stability boundary are the limit points. The stability boundary is composed of two curves connected by a cusp point. Although, the buckling mode changes at this point, the proposed technique can successfully pass the cusp point. Table 3 shows the summary of computations. By comparing the magnitudes of contribution terms α_p and α_ε , before and after the cusp point, it can be concluded that the contribution terms of the load, and the control parameters are relative to the tangent of the stability boundary. Furthermore, the number of iterations in the sixth and seventh increments in comparison with other incremental parts shows that the initial guess of critical eigenvector, which is coming from the previous increment, may only influence the number of iterations when the critical mode changes. Note that, the calculated stability boundary is consistent with the result given by Choong and Kim (2001).

According to Fig. 8, there can be more than one critical load for some values of ε. In such cases, different loading patterns may result in different critical states. For instance, there are three values for P_{cr} when the control parameter ε is equal to 58 N, and they can be reached from the loading patterns **A**, **B** and **C** shown in Fig. 8. In the pattern **A**, first, the control parameter ε relative to the secondary load vector increases from zero to 58 N. Then, the main loading

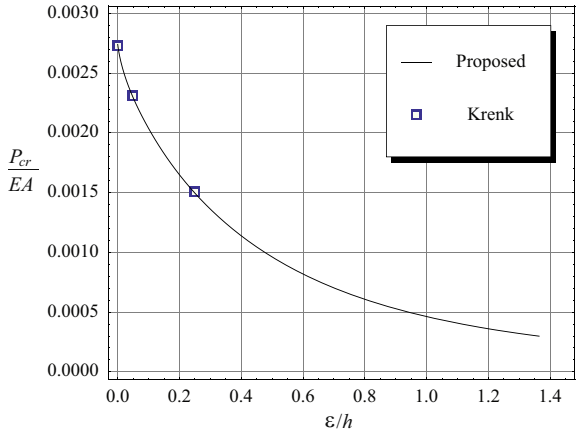

Fig. 6. Stability boundary for the truss-spring system.

Table 1
Analysis of the truss-spring system.

Inc.–Ite.	ε/h	P_{cr}/EA	$\|\|\mathbf{r}_i\|\|/EA$	$\|\|\mathbf{K}_{Ti}\boldsymbol{\Phi}_i\|\| \times L/EA$
1–0	3.92230×10^{-25}	2.74139×10^{-3}	9.57696×10^{-4}	1.25597×10^{-2}
1–1	1.28589×10^{-1}	1.88146×10^{-3}	9.67577×10^{-5}	1.21754×10^{-3}
1–2	1.31609×10^{-1}	1.90284×10^{-3}	3.62082×10^{-6}	1.92554×10^{-5}
1–3	1.31665×10^{-1}	1.89976×10^{-3}	7.66926×10^{-10}	1.25305×10^{-8}
1–4	1.31665×10^{-1}	1.89976×10^{-3}	6.71926×10^{-16}	4.28941×10^{-15}
1–5	1.31665×10^{-1}	1.89976×10^{-3}	3.74114×10^{-29}	5.94289×10^{-28}
2–0	4.48011×10^{-1}	6.04418×10^{-4}	1.38469×10^{-3}	1.32389×10^{-2}
2–1	5.27649×10^{-1}	9.07658×10^{-4}	9.55839×10^{-6}	1.17692×10^{-3}
2–2	5.21600×10^{-1}	9.28282×10^{-4}	5.42059×10^{-8}	1.09304×10^{-5}
2–3	5.21516×10^{-1}	9.28357×10^{-4}	2.16802×10^{-11}	1.36431×10^{-9}
2–4	5.21516×10^{-1}	9.28357×10^{-4}	1.31421×10^{-18}	2.21607×10^{-17}
2–5	5.21516×10^{-1}	9.28357×10^{-4}	5.28680×10^{-34}	1.13687×10^{-32}
3–0	9.38326×10^{-1}	2.97641×10^{-4}	1.88213×10^{-4}	4.79304×10^{-3}
3–1	9.41390×10^{-1}	4.99473×10^{-4}	6.58491×10^{-7}	2.78814×10^{-5}
3–2	9.41713×10^{-1}	4.99436×10^{-4}	2.15160×10^{-8}	1.61726×10^{-7}
3–3	9.41711×10^{-1}	4.99433×10^{-4}	3.74091×10^{-14}	4.50000×10^{-13}
3–4	9.41711×10^{-1}	4.99433×10^{-4}	3.94967×10^{-25}	3.44157×10^{-24}
4–0	1.36160×10^{0}	2.19545×10^{-4}	3.07463×10^{-4}	3.68838×10^{-3}
4–1	1.35945×10^{0}	3.01055×10^{-4}	1.31400×10^{-6}	4.12953×10^{-5}
4–2	1.35964×10^{0}	3.00401×10^{-4}	1.45516×10^{-8}	7.87764×10^{-8}
4–3	1.35964×10^{0}	3.00400×10^{-4}	9.31483×10^{-14}	3.59446×10^{-13}
4–4	1.35964×10^{0}	3.00400×10^{-4}	4.40541×10^{-25}	1.82584×10^{-24}

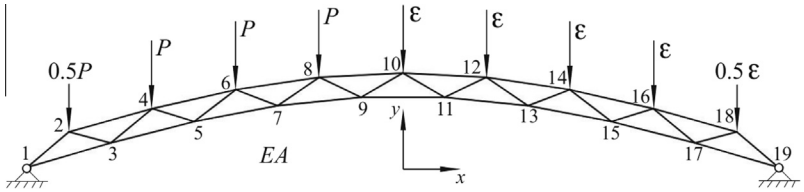

Fig. 7. Plane truss arch.

Table 2
Coordinates of nodes for the plane truss arch.

Nodal No.	x coordinates (cm)	y coordinates (cm)
19, 1	±342.9	0.0
18, 2	±304.8	5.065
17, 3	±266.7	3.475
16, 4	±228.6	8.382
15, 5	±190.5	6.530
14, 6	±152.4	11.085
13, 7	±114.3	8.799
12, 8	±76.2	12.850
11, 9	±38.1	10.005
10	0.0	13.462

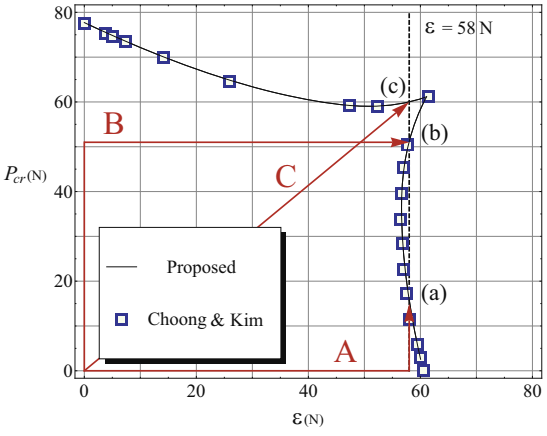

Fig. 8. Stability boundary for the plane truss arch.

is applied until the loading pattern intersects the stability boundary. In **B**, the sequence of loadings is vice versa. The ratio between the load and the control parameters is constant during loading in the loading pattern **C**. Fig. 9 draws the deformed shape of the structure at these critical states.

5.3. Half-sine shallow arch

In this example, the stability boundary of a half-sine pin-ended shallow arch under a concentrated vertical loading P^* is investigated (Fig. 10). The Young's modulus and thermal expansion coefficient are denoted by E and α^*, respectively. A is the area, and I represents the moment of inertia of the cross section.

In order to theoretically analyze the arch, the following assumptions are needed (Chen and Yang, 2007a; Xu et al., 2002): (a) the range of displacements and curvatures is small; (b) the axial force is constant over the span L; and (c) out-of-plane deflections are neglected. For convenience, some variables are changed into the dimensionless form (Chen et al., 2009; Chen and Yang, 2007b; Plaut and Johnson, 1981):

$$u = \frac{1}{r}y, \quad h = \frac{1}{r}h^*, \quad P = \frac{2L^3}{\pi^4 EI r}P^*, \quad \alpha = \frac{L^2}{\pi^2\, r^2}\alpha^*. \tag{50}$$

Here, r represents the radius of gyration of the cross section ($r = \sqrt{I/A}$), and h^* is the rise of the arch. It can be proven that the exact fundamental equilibrium path is implicitly derived from Eqs. (51) and (52) for some values of η (Moghaddasie and Stanciulescu, 2013b):

$$\Delta u_{\text{Mid}} = -\left(\frac{P-h}{1+\eta}+h\right) - P\kappa_{2,1}(\eta), \tag{51}$$

Table 3
Analysis of the plane truss arch.

Increment	No. of iterations	Contributions of terms			Control par. ε (N)	Critical load P_{cr} (N)
		α_u (cm^{-1})	α_p (N^{-1})	α_ε (N^{-1})		
1	4	1.423×10^{-1}	5.038×10^{-1}	8.520×10^{-1}	1.059×10^{1}	7.184×10^{1}
2	4	1.428×10^{-1}	4.537×10^{-1}	8.796×10^{-1}	2.108×10^{1}	6.686×10^{1}
3	4	1.478×10^{-1}	3.919×10^{-1}	9.081×10^{-1}	3.140×10^{1}	6.291×10^{1}
4	4	1.595×10^{-1}	3.111×10^{-1}	9.369×10^{-1}	4.149×10^{1}	6.017×10^{1}
5	5	1.840×10^{-1}	1.960×10^{-1}	9.632×10^{-1}	5.134×10^{1}	5.904×10^{1}
6	7	2.438×10^{-1}	5.148×10^{-3}	9.698×10^{-1}	6.108×10^{1}	6.114×10^{1}
7	10	7.893×10^{-1}	3.566×10^{-1}	4.999×10^{-1}	5.676×10^{1}	4.143×10^{1}
8	4	1.643×10^{-1}	9.853×10^{-1}	4.660×10^{-2}	5.671×10^{1}	3.179×10^{1}
9	4	1.443×10^{-1}	9.890×10^{-1}	3.177×10^{-2}	5.732×10^{1}	2.219×10^{1}
10	4	1.346×10^{-1}	9.868×10^{-1}	8.972×10^{-2}	5.843×10^{1}	1.256×10^{1}
11	4	1.299×10^{-1}	9.821×10^{-1}	1.364×10^{-1}	5.997×10^{1}	2.895×10^{0}

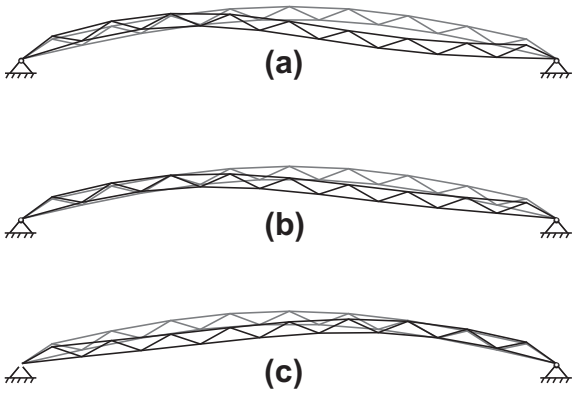

Fig. 9. Deformed shape at critical states corresponding to loading patterns: (a) A (b) B (c) C.

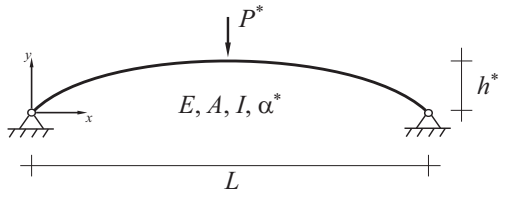

Fig. 10. Half-sine shallow arch.

$$\eta = -\alpha\ \Delta T - \frac{h^2}{4} + \frac{(P-h)^2}{4(1+\eta)^2} + \frac{P^2}{4}\kappa_{2,2}(\eta), \tag{52}$$

where

$$\kappa_{M,N}(\eta) = \sum_{i=1}^{\infty} \frac{1}{(2i+1)^M \left((2i+1)^2+\eta\right)^N}. \tag{53}$$

ΔT shows the temperature change, and Δu_{Mid} is the dimensionless displacement at the midpoint. Along the fundamental equilibrium path, the displacement field is always symmetric. Based on the magnitude of the independent dimensionless parameters h and $\alpha\ \Delta T$, there can be a set of bifurcation points on the fundamental equilibrium path. On the bifurcated paths, an asymmetric buckling mode is added to the symmetric displacement field. The relationship between the external load and the displacement of the midpoint for the bifurcated equilibrium path is as follows (Moghaddasie and Stanciulescu, 2013b):

$$\Delta u_{\text{Mid}} = \frac{P-h}{3} - h - P\left(\frac{1}{3} - \frac{\pi^2}{32}\right). \tag{54}$$

Fig. 11 illustrates the fundamental and the bifurcated equilibrium paths (respectively, denoted by solid and dashed lines) for (a) $h = 4.25$ and (b) $h = 6.0$ with $\alpha\Delta T = 0$.

As it is observed, on the fundamental equilibrium path, there are both limit and bifurcation points. Eqs. (52) and (55) implicitly describe the relationship between the magnitude of critical load corresponding to limit points and the independent parameters h and $\alpha\Delta T$ (Moghaddasie and Stanciulescu, 2013b):

$$1 + \frac{(P_{cr}-h)^2}{2(1+\eta)^3} + \frac{P_{cr}^2}{2}\kappa_{2,3}(\eta) = 0. \tag{55}$$

Furthermore, the locus of bifurcation points in the space of $P_{cr}, h, \alpha\Delta T) \in \mathbb{R}^3$ has the following form:

$$\alpha\Delta T + \frac{h^2}{4} - 4 - \frac{(P_{cr}-h)^2}{12} - \frac{P_{cr}^2}{4}\left(\frac{3\pi^2}{256} - \frac{1}{9}\right) = 0. \tag{56}$$

The authors' technique is applied to two fixed values of the dimensionless rise of the arch ($h = 4.25$ and $h = 6.0$). For this purpose, 20 Timoshenko beam elements with large transverse displacement (Felippa, 2012) are used to discretize the arch. In this example, the control parameter is assumed as $\alpha\Delta T$, and the stability boundaries relative to the first limit and bifurcation points along the equilibrium path are calculated separately. For all analyses, $\Delta s = 3.0$. Fig. 12 draws the stability boundaries given by the half-sine shallow arch theory and the suggested scheme for $h = 4.25$ and $h = 6.0$. The average number of iterations per increment is 4.083. In this figure, the limit and bifurcation points computed by the proposed procedure are denoted by squares and crosses, respectively. As it can be seen, the locus of these points is consistent with the result of the half-sine shallow arch theory.

5.4. Deep clamed arch

A circular deep arch is illustrated in Fig. 13. The arch is clamped at supports and subjected to a concentrated load P at the midpoint (Battini et al., 2003; Wriggers and Simo, 1990). In addition, a bending moment located at the midpoint is considered. The magnitude of this moment increases by the control parameter ε.

This structure includes only limit points along its equilibrium path. For $\varepsilon = 0$, the value of the critical load P_{cr} is equal to 972.73. The corresponding vertical displacement at the top equals $u_{cr} = 72.136$, which shows a highly pre-critical nonlinearity. Fig. 14 draw the deformed shape of the deep clamped arch for three values of ε.

In order to obtain a relationship between the load-bearing capacity of the arch and the control parameter, the authors' technique is used. In this way, the arch is discretized by 20 Timoshenko beam elements with large transverse displacement (Felippa, 2012). Each element includes six degrees of freedom, and both axial and

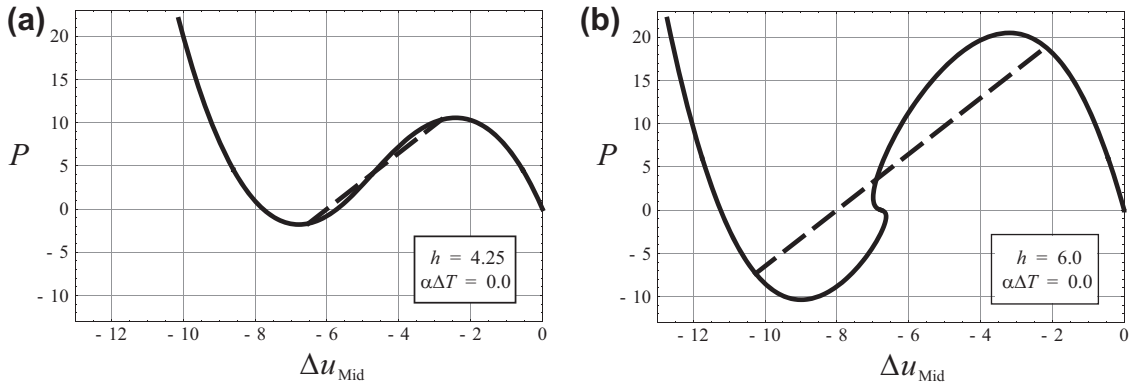

Fig. 11. Equilibrium paths for $\alpha\Delta T = 0.0$ and (a) $h = 4.25$ (b) $h = 6.0$.

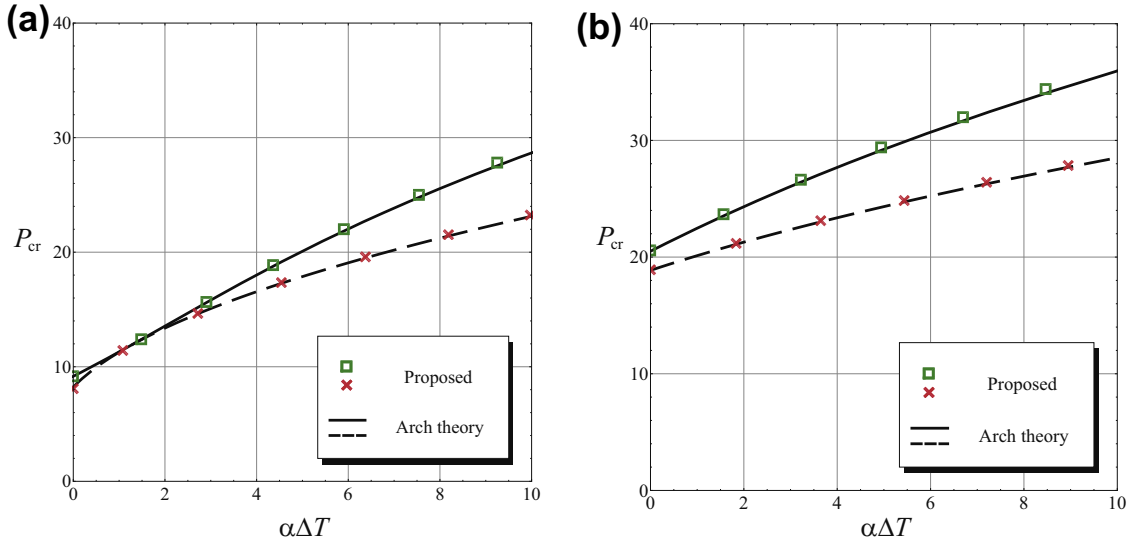

Fig. 12. Stability boundary for the half-sine shallow arch for (a) $h = 4.25$ (b) $h = 6.0$.

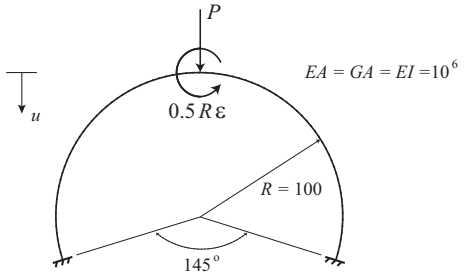

Fig. 13. Deep clamped arch.

shear Green's strains are considered. A summary of the calculation for $\Delta s = 50.0$ is given in Table 4. The analysis is performed within 15 increments and 80 iterations. Fig. 15 illustrates the locus of critical points obtained by the proposed method. Furthermore, four equilibrium paths corresponding to $\varepsilon = 0, 500, 700, 852.8$ are shown. For this part of analysis, first, the bending moment is applied, and then the load P increases from zero. As it can be seen, the limit points vanish when ε reaches the magnitude of 852.8. For higher values of the control parameter, there will be no critical point on the equilibrium path. In this state, the proposed method becomes divergent for larger ε. Fig. 14(c) shows the deformed shape of the arch at critical loadings for $\varepsilon = 852.8$.

The relationship between the time of the analysis and the number of degrees of freedom (DoFs) can be a suitable criterion for evaluating the computational efficiency of the proposed method. For this purpose, the deep clamped arch is discretized by 20, 40, 80 and 160 beam elements and analyzed by (a) the cylindrical arc-length procedure (to trace the equilibrium path) and (b) the suggested approach (to obtain the stability boundary). One can

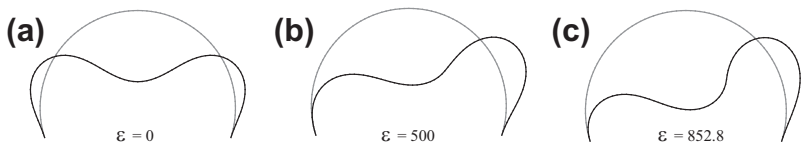

Fig. 14. Deformation of the arch at critical loadings for (a) $\varepsilon = 0$ (b) $\varepsilon = 500$ (c) $\varepsilon = 852.8$.

Table 4
Analysis of the deep clamped arch.

Increment	No. of iterations	Control parameter ε	Critical load P_{cr}	Critical Displacement u_{cr}
1	5	5.3769×10^{1}	9.7040×10^{2}	7.2056×10^{1}
2	6	1.0760×10^{2}	9.6355×10^{2}	7.1807×10^{1}
3	6	1.6146×10^{2}	9.5257×10^{2}	7.1375×10^{1}
4	6	2.1534×10^{2}	9.3793×10^{2}	7.0758×10^{1}
5	5	2.6928×10^{2}	9.2006×10^{2}	6.9969×10^{1}
6	5	3.2337×10^{2}	8.9929×10^{2}	6.9038×10^{1}
7	5	3.7764×10^{2}	8.7590×10^{2}	6.8001×10^{1}
8	5	4.3213×10^{2}	8.5010×10^{2}	6.6904×10^{1}
9	5	4.8682×10^{2}	8.2206×10^{2}	6.5795×10^{1}
10	5	5.4168×10^{2}	7.9198×10^{2}	6.4734×10^{1}
11	6	5.9667×10^{2}	7.6004×10^{2}	6.3792×10^{1}
12	5	6.5176×10^{2}	7.2646×10^{2}	6.3067×10^{1}
13	5	7.0693×10^{2}	6.9152×10^{2}	6.2716×10^{1}
14	5	7.6221×10^{2}	6.5559×10^{2}	6.3047×10^{1}
15	6	8.1779×10^{2}	6.1927×10^{2}	6.5034×10^{1}

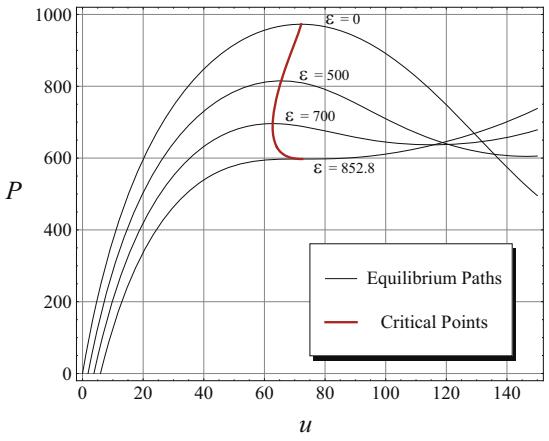

Fig. 15. Equilibrium paths and critical points of the deep clamped arch.

assume that the time of the analysis and the number of DoFs have the following relationship:

$$(\text{Time}) \simeq \alpha \times (\text{DoF})^{\beta}, \tag{57}$$

where, the coefficient α is relative to the computer configuration and other parameters which are not of interest here. The coefficient β shows the increase rate in the number of operations due to the increase in the number of DoFs. Eq. (57) can be rewritten in a logarithmic form:

$$\log\ (\text{Time}) \simeq \log \alpha + \beta\ \log\ (\text{DoF}). \tag{58}$$

Here, β represents the slope of the line in the logarithmic scale.

As it is mentioned, two series of analyses are performed for the deep clamped arch which is simulated by 20, 40, 80 and 160 elements (including 57, 117, 237 and 477 degrees of freedom, respectively). First, the cylindrical arc-length procedure is applied to trace the equilibrium path for 60 incremental and iterative steps. This analysis is accompanied by a critical test function. Here, since the equilibrium path includes simple critical points, the determinant of the tangent stiffness matrix is considered as a test function. Fig. 16 presents the result of the cylindrical arc-length procedure accompanied by the test function. The slope of the regression line is $\beta = 2.25$. The second analysis is performed by the proposed method to trace the stability boundary for 60 incremental and iterative steps. The slope of the regression line is close to the other analysis and equals $\beta = 2.37$. Consequently, the increase rate in the computational cost of the proposed technique is appropriate and comparable with Newton-like procedures which are used for obtaining the equilibrium path.

5.5. Compressed plate

Fig. 17 shows a rectangular plate subjected to a compressive distributed load in the direction of x. All four edges are simply supported. The material and the geometrical properties are given in the figure.

Based on the plate theory, the critical load parameter P_{cr} is as follows (Eriksson and Pacoste, 2002; Eriksson et al., 1999):

$$P_{cr} = P_0 \left(\frac{i^2}{\lambda^2} + \frac{\lambda^2}{i^2} + 2 \right), \tag{59}$$

where $\lambda = L_x/L_y$, and

$$P_0 = \frac{\pi^2 E}{12(1-\nu^2)} \left(\frac{t}{L_y} \right)^2. \tag{60}$$

The minimum value for P_{cr} is equal to $4P_0$ and obtained for $\lambda = i$.

The authors' procedure is applied to trace the stability boundaries corresponding to the first three buckling modes ($i = 1, 2, 3$) separately. In this way, 12×12 plate elements which are satisfying the Kirchhoff hypothesis (Reddy, 2004) (with four nodes and 20 degrees of freedom) are used to discretize the plate. By considering the Kirchhoff hypothesis, the Green's strains become von Kármán strains for the supposed plate elements. The total number of DoFs is 795. Here, the control parameter is assumed as λ. Fig. 18 compares the stability boundaries calculated by the suggested procedure and the plate theory. In this example, $\Delta s = 100.0$, and the average number of iterations per increment is equal to 3.00 for all three analyses. Crosses, triangles and squares denote the

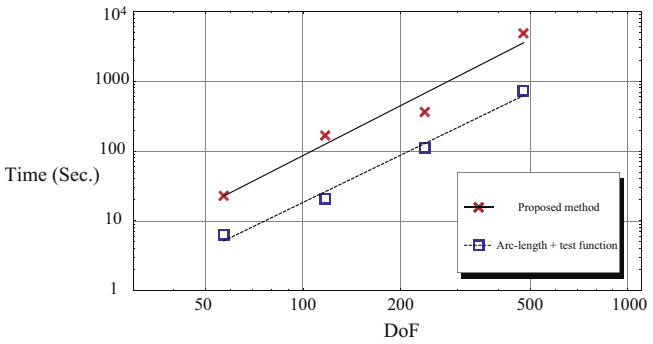

Fig. 16. Relationship between the time of the analysis and the number of DoFs.

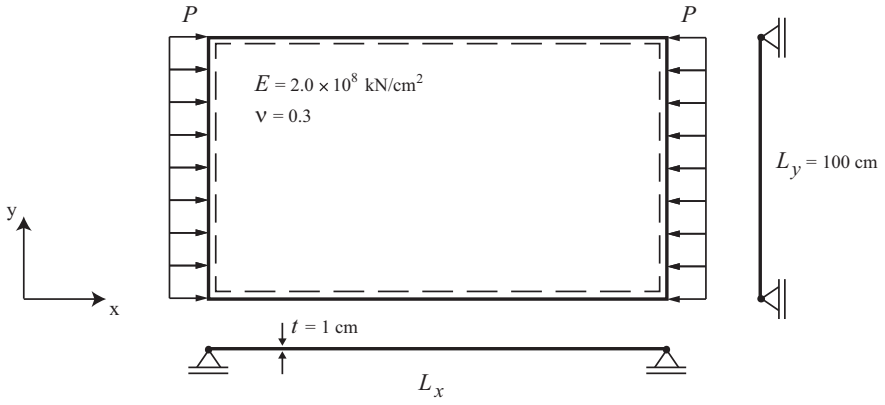

Fig. 17. Compressed plate.

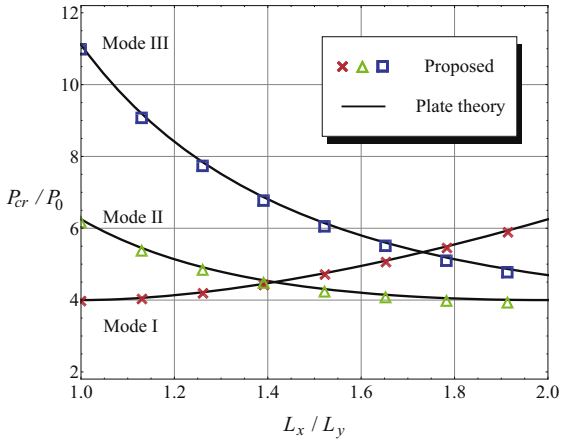

Fig. 18. Stability boundary for the compressed plate.

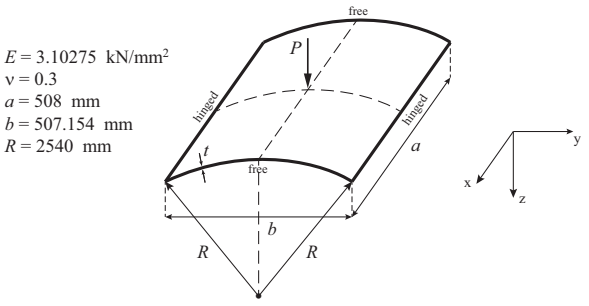

Fig. 20. Cylindrical shell.

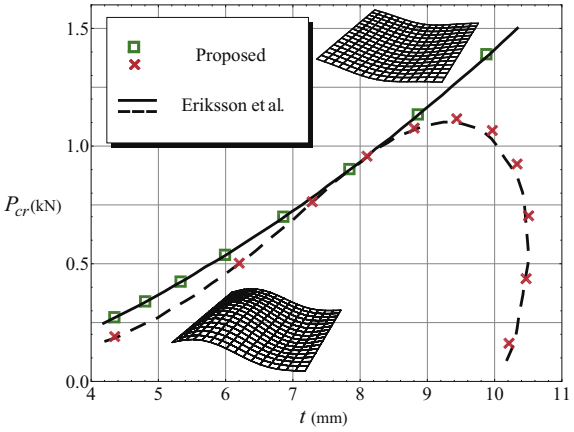

Fig. 21. Stability boundary for the cylindrical shell.

obtained critical points corresponding to the buckling Mode, I, II and III, respectively. In addition, Fig. 18 shows that the suggested method can pass the intersecting points of stability boundaries successfully. Needless to say, these types of points are multi-critical. The critical mode shapes at the ratio $L_x/L_y = 1$ are given in Fig. 19.

5.6. Cylindrical shell

In this example, a shell structure, which is often discussed in the literature (Cho et al., 1998; Deml and Wunderlich, 1997; Eriksson, 1991), is investigated. The structure is a cylindrical shell subjected to a concentrated load at the central point. Fig. 20 illustrates the material and geometrical properties of the shell. The curved edges are free, while the longitudinal ones are hinged.

The magnitude of the critical load can be affected by the variation in the thickness of the shell. In order to trace the stability boundary by the proposed method, 16 × 16 shell elements based on the Kirchhoff–Love kinematic hypothesis (with four nodes and 20 degrees of freedom) are used to discretize the structure. By considering the Kirchhoff–Love kinematic hypothesis, the Green's strains become simpler for the shell element (Reddy, 2004). The

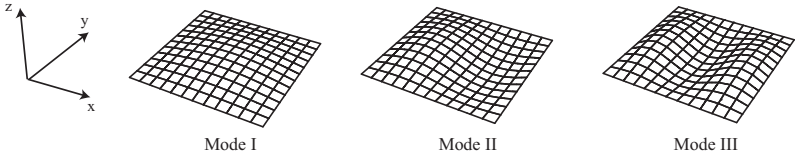

Fig. 19. Critical mode shapes of the compressed plate at $L_x/L_y = 1$.

Table 5
Convergence of the proposed method at the sixth increment of the limit point analysis.

Iteration	t (mm)	P_{cr} (kN)	$\|\|\mathbf{r}_i\|\|$ (kN)	$\|\|\mathbf{K}_{T\ i}\mathbf{\Phi}_i\|\|$ (kN/mm)
0	8.847902	1.118419	7.50491×10^{1}	2.48940×10^{-2}
1	8.882219	1.138058	1.09981×10^{0}	1.01180×10^{-3}
2	8.862555	1.133285	1.35253×10^{-2}	4.42655×10^{-6}
3	8.862363	1.133244	2.53943×10^{-6}	7.24546×10^{-10}
4	8.862363	1.133244	3.23121×10^{-14}	1.00333×10^{-17}
5	8.862363	1.133244	3.59854×10^{-30}	1.21980×10^{-33}

total number of DoFs is 1343. Here, the control parameter is assumed as the thickness t, and the analysis starts from $t_0 = 4.35$ mm. Fig. 21 shows the computed stability boundaries.

As it can be observed, two types of boundaries relative to limit and bifurcation points (denoted by squares and crosses, respectively) are obtained. The corresponding critical mode shapes are drawn in this figure. The suggested procedure is used for tracing limit points with $\Delta s = 2.5$ and bifurcation points with $\Delta s = 12.5$. In addition, the average numbers of iterations per increments are, respectively, 4.57 and 4.30. The calculated stability boundaries are in good agreement with the results given by (Eriksson et al., 1999). Needless to say, the proposed method is less sensitive to variations in the tangent stiffness matrix and has better convergence properties than the other technique.

Two stability boundaries are become tangent at $t \simeq 8$ mm which is called a hilltop branching point (Eriksson, 1997; Eriksson et al., 1999). The proposed technique can successfully pass this multi-critical point with *a quadratic rate of convergence* in the analysis of both limit and bifurcation points. Tables 5 and 6 demonstrate the quadratic convergence behavior at the increments which pass the hilltop branching point.

6. Conclusions

The parameter sensitivity analysis can help the analyst to have better understanding of the structural behavior. Parameters, such as initial geometric defects, additional external loadings and variations in temperature can affect the load carrying capacity of structures. In this paper, the stability of two-parameter elastic structures is investigated. In this way, a new formulation to trace the stability boundary is introduced. Critical points are directly computed from the previous one through an incremental–iterative procedure. In this formulation, the equilibrium condition and the critical constraint are satisfied simultaneously. Furthermore, a spherical arc-length constraint is added to the governing equations. The authors also present a process to update this constraint, which improves the convergence properties. The suggested technique is based on Newton's method which assures a quadratic rate of convergence.

The proposed procedure can trace both limit and simple bifurcation points. It is also extensible for multi-parameter systems by adding extra constraints. The numerical examples show the efficiency of the suggested technique for a variety of structural systems having different types of control parameters and imperfections, such as geometric defects, load imperfections and thermal stresses. For all cases, the authors' method obtains the stability boundary for a wide range of the control parameter with high accuracy and appropriate computational efficiency.

References

Battini, J.M., Pacoste, C., Eriksson, A., 2003. Improved minimal augmentation procedure for the direct computation of critical points. Comput. Methods Appl. Mech. Eng. 192, 2169–2185.

Bergan, P.G., 1980. Solution algorithms for nonlinear structural problems. Comput. Struct. 12, 497–509.

Cardona, A., Huespe, A., 1999. Evaluation of simple bifurcation points and post-critical path in large finite rotation problems. Comput. Methods Appl. Mech. Eng. 175, 137–156.

Casciaro, R., Salerno, G., Lanzo, A.D., 1992. Finite element asymptotic analysis of slender elastic structures: a simple approach. Int. J. Numer. Methods Eng. 35, 1397–1426.

Casciaro, R., Garcea, G., Attanasio, G., Giordano, F., 1998. Perturbation approach to elastic post-buckling analysis. Comput. Struct. 66, 585–595.

Chen, H., Blandford, G.E., 1993. Work-increment-control method for non-linear analysis. Int. J. Numer. Methods Eng. 36, 909–930.

Chen, J.S., Yang, C.H., 2007a. Experiment and theory on the nonlinear vibration of a shallow arch under harmonic excitation at the end. ASME J. Appl. Mech. 74, 1061–1070.

Chen, J.S., Yang, M.R., 2007b. Vibration and stability of a shallow arch under a moving mass-dashpot-spring system. ASME J. Vib. Acoust. 129, 66–72.

Chen, J.S., Ro, W.C., Lin, J.S., 2009. Exact static and dynamic critical loads of a sinusoidal arch under a point force at the midpoint. Int. J. Non Linear Mech. 44, 66–70.

Cho, C., Park, H.C., Lee, S.W., 1998. Stability analysis using a geometrically nonlinear assumed strain solid shell element model. Finite Elem. Anal. Des. 29, 121–135.

Choong, K.K., Kim, J.Y., 2001. A numerical strategy for computing the stability boundaries for multi-loading systems by using generalized inverse and continuation method. Eng. Struct. 23, 715–724.

Crisfield, M.A., 1981. A fast incremental/iterative solution procedure that handles "snap-through". Comput. Struct. 13, 55–62.

Crisfield, M.A., 1983. An arc-length method including line searches and accelerations. Int. J. Numer. Methods Eng. 19, 1269–1289.

Crisfield, M.A., 1991. Non-linear Finite Element Analysis of Solids and Structures. Essentials, vol. 1. J. Wiley and Sons, Chichester.

Crisfield, M.A., 1997. Non-linear Finite Element Analysis of Solids and Structures. Advanced Topics. J. Wiley and Sons, Chichester.

de Souza Neto, E.A., Feng, Y.T., 1999. On the determination of the path direction for arc-length methods in the presence of bifurcations and 'snap-backs'. Comput. Methods Appl. Mech. Eng. 179, 81–89.

Deml, M., Wunderlich, W., 1997. Direct evaluation of the 'worst' imperfection shape in shell buckling. Comput. Methods Appl. Mech. Eng. 149, 201–222.

Dennis Jr., J.E., Schnabel, R.B., 1996. Numerical Methods for Unconstrained Optimization and Nonlinear Equations. Society for Industrial Mathematics.

Eriksson, A., 1991. Derivatives of tangential stiffness matrices for equilibrium path descriptions. Int. J. Numer. Methods Eng. 32, 1093–1113.

Eriksson, A., 1994. Fold lines for sensitivity analyses in structural instability. Comput. Methods Appl. Mech. Eng. 114, 77–101.

Eriksson, A., 1997. Equilibrium subsets for multi-parametric structural analysis. Comput. Methods Appl. Mech. Eng. 140, 305–327.

Eriksson, A., Pacoste, C., 2002. Element formulation and numerical techniques for stability problems in shells. Comput. Methods Appl. Mech. Eng. 191, 3775–3810.

Eriksson, A., Pacoste, C., Zdunek, A., 1999. Numerical analysis of complex instability behaviour using incremental–iterative strategies. Comput. Methods Appl. Mech. Eng. 179, 265–305.

Felippa, C.A., 2012. Nonlinear finite element methods. <http://www.colorado.edu/engineering/CAS/courses.d/NFEM.d/Home.html>.

Forde, B.W.R., Stiemer, S.F., 1987. Improved arc length orthogonality methods for nonlinear finite element analysis. Comput. Struct. 27, 625–630.

Fujii, F., Okazawa, S., 1997. Pinpointing bifurcation points and branch-switching. ASCE J. Eng. Mech. 123, 179–189.

Fujii, F., Ramm, E., 1997. Computational bifurcation theory: path-tracing, pinpointing and path-switching. Eng. Struct. 19, 385–392.

Garcea, G., Salerno, G., Casciaro, R., 1999. Extrapolation locking and its sanitization in Koiter's asymptotic analysis. Comput. Methods Appl. Mech. Eng. 180, 137–167.

Table 6
Convergence of the proposed method at the fourth increment of the bifurcation point analysis.

Iteration	t (mm)	P_{cr} (kN)	$\|\|\mathbf{r}_i\|\|$ (kN)	$\|\|\mathbf{K}_{T\ i}\mathbf{\Phi}_i\|\|$ (kN/mm)
0	8.197937	9.920150×10^{-1}	1.01126×10^{2}	1.61170×10^{0}
1	8.104908	9.572046×10^{-1}	3.57179×10^{0}	5.62838×10^{-2}
2	8.101980	9.569087×10^{-1}	8.40852×10^{-3}	1.95184×10^{-4}
3	8.101974	9.569080×10^{-1}	5.46225×10^{-8}	1.57205×10^{-9}
4	8.101974	9.569080×10^{-1}	2.61916×10^{-15}	5.84605×10^{-20}

Garcea, G., Madeo, A., Zagari, G., Casciaro, R., 2009. Asymptotic post-buckling FEM analysis using corotational formulation. Int. J. Solids Struct. 46, 377–397.
Godoy, L.A., Banchio, E.G., 2001. Singular perturbations for sensitivity analysis in symmetric bifurcation buckling. Int. J. Numer. Methods Eng. 52, 1465–1485.
Huseyin, K., 1975. Nonlinear Theory of Elastic Stability. Noordhoff.
Ibrahimbegović, A., Al Mikdad, M., 2000. Quadratically convergent direct calculation of critical points for 3d structures undergoing finite rotations. Comput. Methods Appl. Mech. Eng. 189, 107–120.
Ikeda, K., Ohsaki, M., 2007. Generalized sensitivity and probabilistic analysis of buckling loads of structures. Int. J. Non Linear Mech. 42, 733–743.
Koiter, W.T., 1945. On the stability of elastic equilibrium (Ph.D. Dissertation). Delft University of Technology, Delft, Holland.
Kouhia, R., Tůma, M., Mäkinen, J., Fedoroff, A., Marjamäki, H., 2012. Implementation of a direct procedure for critical point computations using preconditioned iterative solvers. Comput. Struct. 108, 110–117.
Krenk, S., 1995. An orthogonal residual procedure for non-linear finite element equations. Int. J. Numer. Methods Eng. 38, 823–839.
Krenk, S., 2009. Non-linear Modeling and Analysis of Solids and Structures. Cambridge University Press.
Lam, W.F., Morley, C.T., 1992. Arc-length method for passing limit points in structural calculation. J. Struct. Eng. 118, 169–185.
Le Grognec, P., Le Van, A., 2008. Elastoplastic bifurcation and collapse of axially loaded cylindrical shells. Int. J. Solids Struct. 45, 64–86.
Lopez, S., 2002a. Detection of bifurcation points along a curve traced by a continuation method. Int. J. Numer. Methods Eng. 53, 983–1004.
Lopez, S., 2002b. Post-critical analysis of structures with a nonlinear pre-buckling state in the presence of imperfections. Comput. Methods Appl. Mech. Eng. 191, 4421–4440.
Magnusson, A., Svensson, I., 1998. Numerical treatment of complete load–deflection curves. Int. J. Numer. Methods Eng. 41, 955–971.
Moghaddasie, B., Stanciulescu, I., 2013a. Direct calculation of critical points in parameter sensitive systems. Comput. Struct. 117, 34–47.
Moghaddasie, B., Stanciulescu, I., 2013b. Equilibria and stability boundaries of shallow arches under static loading in a thermal environment. Int. J. Non Linear Mech. 51, 132–144.
Moore, G., Spence, A., 1980. The calculation of turning points of nonlinear equations. SIAM J. Numer. Anal. 17, 567–576.
Ohsaki, M., 2005. Design sensitivity analysis and optimization for nonlinear buckling of finite-dimensional elastic conservative structures. Comput. Methods Appl. Mech. Eng. 194, 3331–3358.
Ohsaki, M., Ikeda, K., 2009. Imperfection sensitivity of degenerate hilltop branching points. Int. J. Non Linear Mech. 44, 324–336.
Parente Jr., E., de Holanda, A.S., da Silva, S.M.B.A., 2006. Tracing nonlinear equilibrium paths of structures subjected to thermal loading. Comput. Mech. 38, 505–520.
Parente Jr., E., de Sousa Jr., J.B.M., 2008. Design sensitivity analysis of nonlinear structures subjected to thermal loads. Comput. Struct. 86, 1369–1384.
Planinc, I., Saje, M., 1999. A quadratically convergent algorithm for the computation of stability points: the application of the determinant of the tangent stiffness matrix. Comput. Methods Appl. Mech. Eng. 169, 89–105.
Plaut, R.H., Johnson, E.R., 1981. The effects of initial thrust and elastic foundation on the vibration frequencies of a shallow arch. J. Sound Vib. 78, 565–571.
Ramm, E., 1981. Strategies for Tracing the Nonlinear Response near Limit Points. Springer.
Reddy, J.N., 2004. An Introduction to Nonlinear Finite Element Analysis. Oxford University Press, USA.
Rezaiee-Pajand, M., Tatar, M., Moghaddasie, B., 2009. Some geometrical bases for incremental–iterative methods. Int. J. Eng. Trans. B Appl. 22, 245–256.
Riks, E., 1979. An incremental approach to the solution of snapping and buckling problems. Int. J. Solids Struct. 15, 529–551.
Seydel, R., 1979. Numerical computation of branch points in nonlinear equations. Numer. Math. 33, 339–352.
Thompson, J.M.T., Hunt, G.W., 1973. A General Theory of Elastic Stability. J. Wiley.
Vannucci, P., Cochelin, B., Damil, N., Potier-Ferry, M., 1998. An asymptotic–numerical method to compute bifurcating branches. Int. J. Numer. Methods Eng. 41, 1365–1389.
Widjaja, B.R., 1998. Path-following technique based on residual energy suppression for nonlinear finite element analysis. Comput. Struct. 66, 201–209.
Wriggers, P., Simo, J.C., 1990. A general procedure for the direct computation of turning and bifurcation points. Int. J. Numer. Methods Eng. 30, 155–176.
Wriggers, P., Wagner, W., Miehe, C., 1988. A quadratically convergent procedure for the calculation of stability points in finite element analysis. Comput. Methods Appl. Mech. Eng. 70, 329–347.
Wu, B., 2000. Direct calculation of buckling strength of imperfect structures. Int. J. Solids Struct. 37, 1561–1576.
Wu, B., Wang, Z., 1997. A perturbation method for the determination of the buckling strength of imperfection-sensitive structures. Comput. Methods Appl. Mech. Eng. 145, 203–215.
Xu, J.X., Huang, H., Zhang, P.Z., Zhou, J.Q., 2002. Dynamic stability of shallow arch with elastic supports – application in the dynamic stability analysis of inner winding of transformer during short circuit. Int. J. Non Linear Mech. 37, 909–920.